OPTICA

Vernier microcombs for high-frequency carrier envelope offset and repetition rate detection

Kaiyi Wu,[1,†,*] Nathan P. O'Malley,[1,†] Saleha Fatema,[1] Cong Wang,[1,2] Marcello Girardi,[3] Mohammed S. Alshaykh,[4] Zhichao Ye,[3] Daniel E. Leaird,[1,5] Minghao Qi,[1] Victor Torres-Company,[3] and Andrew M. Weiner[1]

[1]Elmore Family School of Electrical and Computer Engineering, Purdue University, West Lafayette, Indiana 47907, USA
[2]Current address: Department of Surgery, Indiana University School of Medicine, Indianapolis, Indiana 46202, USA
[3]Department of Microtechnology and Nanoscience, Chalmers University of Technology, Gothenburg SE-41296, Sweden
[4]Electrical Engineering Department, King Saud University, Riyadh 11421, Saudi Arabia
[5]Current address: Torch Technologies, supporting AFRL/RW, Eglin Air Force Base, Shalimar, Florida 32579, USA
[†]These authors contributed equally to this work.
*wu1871@purdue.edu

Received 1 February 2023; revised 22 April 2023; accepted 24 April 2023; published 18 May 2023

Recent developments in Kerr microcombs may pave the way to a future with fully stabilized ultralow size, weight, and power consumption (SWaP) frequency combs. Nevertheless, Kerr microcombs are still hindered by a bandwidth/repetition rate trade-off. That is, the octave bandwidth needed for self-referencing is typically realized only with ∼THz repetition rates beyond the range of standard commercial photodetectors. The carrier envelope offset frequency f_{CEO} is often likewise too high for detection. Dual-comb techniques for the measurement of THz repetition rates have made exciting progress, but the f_{CEO} detection problem remains largely unaddressed. In this work, utilizing a Vernier dual-comb configuration, we demonstrate simultaneous detection of the electronically divided ∼900 GHz repetition rate and ∼97 GHz carrier envelope offset frequency of an octave-spanning microcomb. This, in turn, could help usher optical atomic clocks, low-noise microwave generators, and optical frequency synthesizers into various real-world applications.

https://doi.org/10.1364/OPTICA.486755

1. INTRODUCTION

Optical frequency combs are integral to the world's most stable clocks [1,2] and lowest-noise microwave generators [3], and they have proven useful for myriad other applications such as optical frequency synthesis [4], LIDAR [5], spectroscopy [6], and astronomy [7]. Some of the optical comb's significance can be attributed to its ability to bridge the optical and RF domains—that is, the frequency of any given comb mode f_m can be written simply as

$$f_m = m \times f_{rep} + f_{CEO}. \quad (1)$$

Here, f_{CEO} denotes the carrier envelope offset (CEO) frequency, which lies between $-f_{rep}/2$ and $+f_{rep}/2$. In many comb generators, f_{rep} is on the order of 10 s of GHz or less [8]. Thus, via the frequency comb equation above, an optical frequency (f_m) can be represented in terms of two RF frequencies (f_{rep} and f_{CEO}). By appropriately controlling either f_m or f_{rep}, one can achieve optical-to-RF or RF-to-optical frequency conversion, respectively [8]. Importantly, however, this does not fully leverage the frequency comb's stability—for the most precise tasks, f_{CEO} must also be stabilized. CEO stabilization was demonstrated in 2000 via f-2f self-referencing and relied on the nonlinear broadening of a mode-locked laser frequency comb to reach an octave span [4,9].

Over the last decade or so, techniques for on-chip generation of frequency combs have developed rapidly, motivated in part by the potential for frequency comb operation in a field-deployable low size, weight, and power consumption (SWaP) package [10]. The first on-chip f-2f self-referenced microcomb with a 16.4 GHz repetition rate relied on nonlinear fibers to coherently broaden the spectrum to an octave [11]. Octave-spanning combs enabling f-2f self-referencing were a key milestone for bulk frequency combs, and the demonstration of the first on-chip octave-spanning coherent combs [12,13] in silicon nitride (SiN) microring resonators was likewise significant. Critically, in order to achieve the stringent requirements for f-2f self-referencing, large intracavity power is needed. This has, in turn, generally limited on-chip octave-spanning combs to small cavities and, therefore, repetition rates on the order of ∼1 THz.

This has led to two significant challenges: first, the repetition rate is far from being electronically detectable. Second, the CEO frequency is often likewise not detectable. The first challenge has been overcome through standard optical division using

a second narrowband, low-repetition rate comb to divide the octave-spanning, high-repetition rate comb. This approach has been demonstrated using a 22 GHz SiO_2 disk resonator [14,15]. Similarly, electro-optic division can be applied as well [16]. Alternatively, a "Vernier" approach featuring two narrowband combs has also been demonstrated toward detecting ∼200 GHz repetition rates [17]. Compared to standard optical division approaches, the Vernier dual-comb scheme uses resonators with smaller radii, thereby reducing the system's footprint. Additionally, higher repetition rate solitons have higher optical power per comb line. This can factor into obtaining higher signal-to-noise beat notes, which are important for many comb systems, but comes at the cost of a sparser spectrum that is less suited to spectroscopic applications. However, the second challenge, namely the difficulty of attaining a detectable CEO frequency, has not been much addressed. A typical solution is fabricating many microresonators, each with slightly different geometrical parameters, in hopes of at least a few devices in a batch having a detectable CEO frequency. This could pose a major roadblock in the eventual field deployment of microcombs.

In this work, we demonstrate a novel method for extending the detectable range of large CEO frequencies using dual SiN-based microresonators. Additionally, we leverage a Vernier strategy to detect the ∼THz repetition rate of an octave-spanning microcomb. We compare both CEO and repetition rate results with out-of-loop measurements using an electro-optic (EO) comb and a stabilized fiber laser comb. While the EO and fiber combs are highly useful for validating our microcomb system performance, they do not offer the potential to reach the same very small footprint as the microcombs.

2. CONCEPTS

The schematics in Figs. 1(a) and 1(b) illustrate our Vernier dual microcomb configuration consisting of a main comb (f_{rep1}, f_{CEO1}) and a Vernier comb (f_{rep2}, f_{CEO2}) with large and slightly offset (∼20 GHz) repetition rates. Excited by a common pump, the dual combs produce two detectable beats, as indicated in Fig. 1(b). One is the difference between the repetition rates,

$$\delta f_{\mathrm{rep}} = f_{\mathrm{rep1}} - f_{\mathrm{rep2}}, \tag{2}$$

detected at the first sideband. The other is the Vernier beat. As a result of the different repetition rates, the two combs walk off from each other and meet again at the Vernier overlap,

$$f_{\mathrm{Vernier}} = n f_{\mathrm{rep1}} - (n+1) f_{\mathrm{rep2}}, \tag{3}$$

where n is the number of lines away from the pump for the main comb. We extend the Vernier approach for repetition rate detection first introduced with narrowband ∼200 GHz combs in [17] to, in this work, ∼THz octave-spanning combs. Electronic frequency division and mixing of the two signals (δf_{rep} and f_{Vernier}) can be used to obtain a divided version of either of the repetition rates,

$$\frac{f_{\mathrm{rep1}}}{n+1} = \delta f_{\mathrm{rep}} - \frac{f_{\mathrm{Vernier}}}{n+1}, \tag{4}$$

$$\frac{f_{\mathrm{rep2}}}{n} = \delta f_{\mathrm{rep}} - \frac{f_{\mathrm{Vernier}}}{n}. \tag{5}$$

Figure 1(a) indicates the simplified experimental configuration for dividing f_{rep1}. Critically, this approach uses only low-frequency ($\delta f_{\mathrm{rep}} < 20$ GHz, $f_{\mathrm{Vernier}} < 10$ GHz) beats to arrive at the repetition rate (normally undetectable) divided down into range for electronic processing.

To measure the CEO frequency, the conventional f-2f self-referencing scheme frequency doubles a comb line at long wavelength via second-harmonic generation (SHG) to beat with another comb line at short wavelength, directly obtaining f_{CEO} [indicated by the blue lines in Fig. 1(c)]. However, the limited bandwidth of typical photodetectors (PDs) may prevent detection of the CEO beat when the CEO frequency is greater than a few tens of GHz. In this paper, we develop a modified f-2f approach which uses sum-frequency generation (SFG), as illustrated in Figs. 1(a) and 1(c), to translate the beat note down to detectable frequencies. Rather than relying on simply doubling a single comb, this SFG process generates multiple nonlinear products resulting from the summation of a single comb line from each comb. Figure 1(c) illustrates the SFG scheme for obtaining the modified f-2f beat. The positions of the SFG lines near the short wavelength comb line are related to the two closest SHG-generated frequency-doubled lines from both main and Vernier combs [blue and orange dotted lines in Fig. 1(c)]. One SFG line will be produced midway between these two SHG lines, as a result of sum-frequency mixing between the two fundamental frequencies giving rise to the SHG lines (green dashed line). Other SFG lines are located at the two sides of this middle line with an equal spacing of δf_{rep}, generated by summing one comb line from the main and Vernier combs, respectively, that are some number of lines away from the SHG fundamental frequencies [various colors, depicted as dashed lines in the 1 μm region (right-most part) of Fig. 1(c)]. This group of lines significantly increases the chance of attaining a detectable f-2f beat (hereafter termed $f_{\mathrm{f-2f}}$) as the short wavelength comb line can beat with the nearest of the densely spaced SFG nonlinear products. The frequency shifting of the $f_{\mathrm{f-2f}}$ beat in the SFG scheme is thus attained by downmixing the high-frequency f_{CEO} with N numbers of δf_{rep}, where N is the number of lines between the Vernier overlap position and the selected main comb line for SFG. We note that, for simplicity and visualization, the schematic in Fig. 1(c) shows a special case where all the illustrated beat notes have positive signs following their definitions in this paper, and the Vernier overlap position is the same as the comb line for conventional SHG approach. However, the relation between the indicated beat notes we are deriving later is not limited to this case.

The resulting f-2f beat can be expressed using f_{CEO}, δf_{rep}, and f_{Vernier}, as indicated in Fig. 1(c) [the detailed derivations can be found in Supplement 1, N represents a division factor defined in Eq. (S13)]:

$$f_{\mathrm{f-2f}} = f_{\mathrm{CEO1}} + f_{\mathrm{Vernier}} - N \times \delta f_{\mathrm{rep}}. \tag{6}$$

We can sum different combinations of comb lines using a periodically poled lithium niobate (PPLN) waveguide with a conversion wavelength range covering the desired short wavelength comb line (usually the short wavelength dispersive wave position with the highest power). We note that the nonlinear products will cover only a particular spectral band with width Δf_{SFG}, and if the short wavelength dispersive wave falls within this band, the minimum beat frequency will not exceed $\delta f_{\mathrm{rep}}/2$ (here <10 GHz), which guarantees a detectable $f_{\mathrm{f-2f}}$. In principle, Δf_{SFG} is set by the long-wavelength comb line powers for the SFG process, and the conversion efficiency and phase matching bandwidth (∼0.4 nm in our experiment) of the PPLN device.

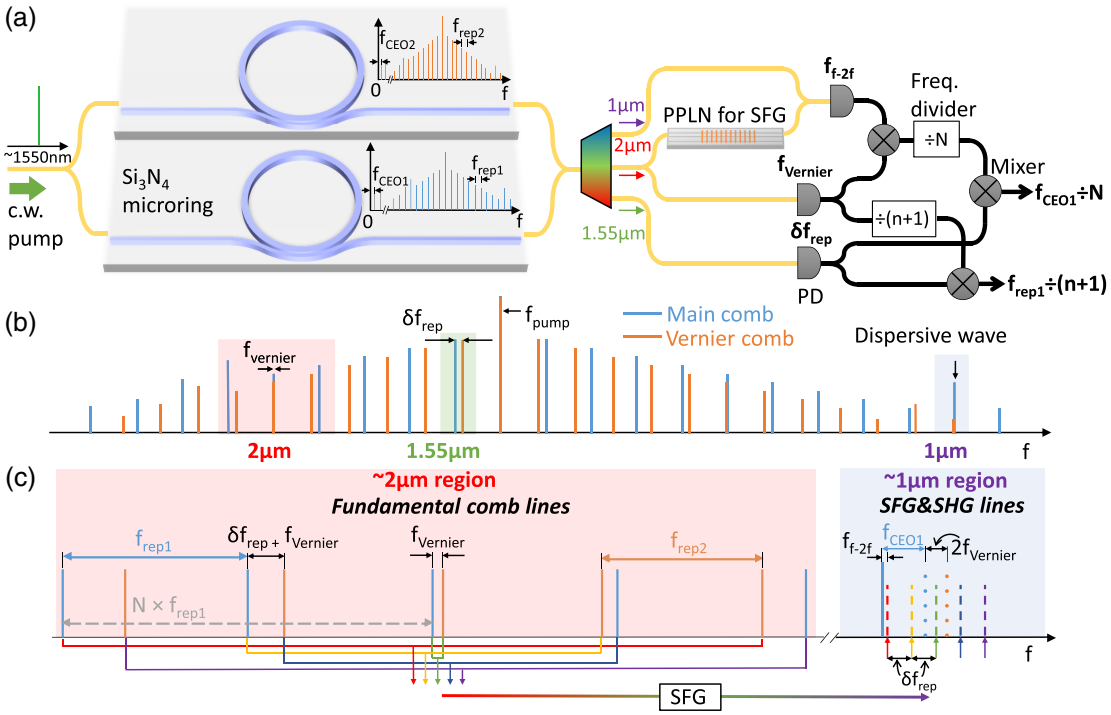

Fig. 1. Schematic of detecting the divided f_{CEO1} and divided f_{rep1} using the Vernier dual-comb approach. (a) Overview of the experimental configuration. (b) Combined dual-comb with highlighted spectral regions for generating and detecting δf_{rep} beat, Vernier beat, and the modified f-2f beat. (c) Zoom-in of the spectral regions for the modified f-2f scheme using sum-frequency generation (SFG) between comb lines from the main and Vernier comb to beat with a short wavelength comb line. The left side of the figure depicts spectral lines from each of the combs (blue and orange, respectively) in the long wavelength (~2 μm) region of the spectrum, centered around the Vernier overlap. The solid horizontal lines at the bottom in various colors, together with the corresponding arrows, indicate the various combinations of comb lines that can mix through SFG to produce a multiplicity of upconverted spectral components spaced by δf_{rep} near a selected short wavelength comb line. The right side of the figure shows the short wavelength spectral region (~1 μm), zooming in on a single comb line of interest (blue solid line; in our experiment, this is the short wavelength dispersive wave from the main comb). The blue and orange dotted lines are SHG products from either the main comb or the Vernier comb respectively, originating in the Vernier overlap region. The dashed lines extended vertically from the solid arrows, drawn in various colors, portray the multiplicity of SFG products. Note that the separation between the blue dotted SHG line and the blue solid comb line is equal to the carrier envelope offset frequency f_{CEO1} for the main comb.

Furthermore, we can acquire the divided CEO frequency beat of the main comb by electronically frequency mixing and dividing the three beats δf_{rep}, $f_{Vernier}$, and f_{f-2f} using Eq. (6),

$$\frac{f_{CEO1}}{N} = \frac{(f_{f-2f} - f_{Vernier})}{N} + \delta f_{rep}. \tag{7}$$

Again, as with the repetition rate acquisition strategy, this approach can allow electronic processing of detectable beats to measure an otherwise-undetectable f_{CEO}. The Vernier approaches for measuring large f_{rep} and f_{CEO} could together enable easier comb stabilization for a variety of applications.

3. EXPERIMENTAL RESULTS

Toward demonstration of this Vernier method, we utilize two high-quality factor Si_3N_4 microring resonators on separate chips fabricated on the same wafer for octave-spanning comb generation enabled by an ultra-smooth Si_3N_4 process described in [18]. We design the ring geometry to achieve dispersive wave emission around 1 μm and 2 μm for the purpose of f-2f self-referencing. The subtractive fabrication process provides a well-controlled Si_3N_4 film thickness of 743 ± 5 nm. The ring widths are designed to be 1630 nm and 1580 nm for the main and Vernier comb, respectively. The main ring with a designed radius of 25.274 μm exhibits a free spectral range (FSR) of ~896 GHz, while the Vernier ring with radius of 25.826 μm shows an FSR of ~876 GHz. To effectively couple the octave-spanning combs with spectra spanning from ~1 μm to ~2 μm, we adopt 620-nm-wide pulley couplers [19], which offer good light extraction at the shorter wavelengths of ~1 μm.

We simultaneously reach the soliton state for both microrings using the rapid laser scanning method [20]. An external cavity diode laser (ECDL) at ~1549 nm is frequency shifted by a single-sideband modulator driven with a voltage-controlled oscillator. The modulated pump is split into two branches and amplified using an erbium-doped fiber amplifier (EDFA) in each arm. We use single-mode lensed fibers for in- and outcoupling to and from the Si_3N_4 chips. The estimated on-chip pump powers for octave-spanning dual-comb generation are ~320 mW for the main comb and ~490 mW for the Vernier comb. We correct for the slight difference between the pump resonances by tuning the stage temperatures controlled by thermoelectric coolers (TECs). The complete experimental setup can be found in Supplement 1. Figure 2(a) shows the optical spectra for main and Vernier combs in single soliton states, measured after a coarse wavelength division multiplexer (CWDM) to reject the strong pump. Both spectra show octave-spanning combs. To the best of our knowledge, this is the first demonstration of dual octave-spanning Kerr combs simultaneously pumped by a single laser. We note that the microring geometry for the main comb is carefully designed to achieve

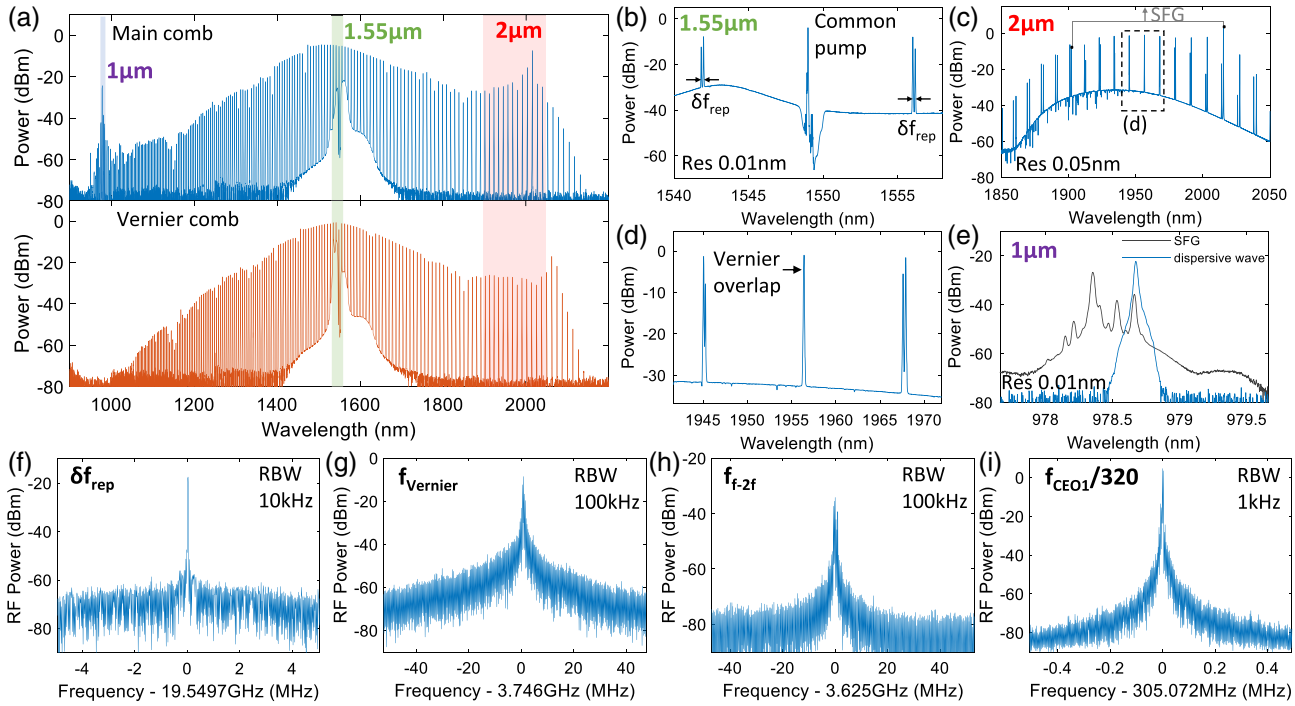

Fig. 2. (a)–(e) Optical spectrum analyzer traces. (a) Main comb (blue) and Vernier comb (orange) after CWDM filters. The three shadow regions indicate the 1 μm (blue), 1.55 μm (green), and 2 μm (red) spectral components being employed. (b) Comb lines at ∼1.55 μm showing the common pump and δf_{rep}. (c) Amplified comb lines at ∼2 μm after the TDFA, at the 25% port of a subsequent 75:25 fiber splitter. (d) Zoom-in view of the dashed region in (c) showing comb lines overlap at the Vernier point at ∼1956 nm. (e) SFG and short wavelength dispersive wave spectra at ∼1 μm. (f)–(i) Electrical spectrum analyzer traces of beat notes. (f) δf_{rep} beat. (g) Vernier beat. (h) f-2f beat. (i) Divided f_{CEO} beat.

dispersive wave emission at ∼1 μm. The Vernier comb, on the other hand, does not need to be octave-spanning as long as the comb covers at least one Vernier period and the longer wavelength spectrum can cover the fundamental SFG wavelengths at ∼2 μm. As a result, the resonator and pulley coupler design for efficient shorter wavelength light generation and extraction of the Vernier comb can be relaxed. The dispersion of the main comb results in a short wavelength dispersive wave at ∼978.67 nm. By fine-tuning the pump frequency after soliton generation, we can reach this dispersive wave state, where we attain the highest power for the short wavelength dispersive wave for the main comb. This is beneficial for the f-2f beat detection. The dispersive wave state for the Vernier comb is not important. The shadowed regions in Fig. 2(a) indicate the three spectral regions for detecting the beat notes. The Vernier overlap appears symmetrically at both sides of the pump spaced by $\sim nf_{rep1}$ (here, $n = 45$), which are at around ∼1.3 μm and ∼2 μm. We choose the one at ∼2 μm to simplify our wavelength division scheme. In our system setup, instead of using the CWDM for pump rejection, which will introduce insertion loss ripples outside the optical communication bands, we use WDM filters to separate the 1 μm, 1.55 μm, and 2 μm spectral components for the main comb and combine with the Vernier comb using two fiber couplers at 1.55 μm and 2 μm.

Figure 2(b) shows the optical spectrum around the pump, where the first sidebands between the dual combs are spaced by δf_{rep}. The 2 μm comb lines are sent to a thulium-doped fiber amplifier (TDFA) (Cybel) to enhance the optical powers, followed by a 75:25 fiber coupler. The spectrum in Fig. 2(c) shows the amplified 2 μm comb lines measured at the 25% port. This port is used for Vernier beat detection. The roll-off in the spectrum below ∼1900 nm and above ∼2020 nm reflects the bandwidth of our TDFA as well as the long-wavelength edge of the microcomb spectrum. Figure 2(d) shows the zoom-in spectrum at the Vernier overlap at ∼1956 nm. The 75% port is sent to a PPLN waveguide (Srico) with a conversion wavelength centered at ∼978.4 nm for the SFG process. The overall conversion efficiency for the PPLN, including in- and outcoupling fibers, is measured to be ∼5%/W using a commercial tunable ECDL (Sacher) at ∼2 μm. Figure 2(e) shows the spectra of SFG (black) and the short wavelength dispersive wave from the main comb (blue) after combining with a fiber coupler, where we obtain reasonable powers of ∼ − 36 dBm for SFG at ∼978.66 nm and ∼ − 22 dBm for the dispersive wave at ∼978.67 nm. Multiple peaks are observed in the SFG spectrum. The desired SFG line closest to the short wavelength dispersive wave is from the summation between ∼2015 nm line (long wavelength dispersive wave) from the main comb and the ∼1902 nm line from the Vernier comb that are five FSRs away from the SHG fundamental frequency at ∼1956 nm, as the gray lines in Fig. 2(c) indicate. The strongest peak at ∼978.35 nm comes from the SHG process of both combs at the Vernier overlap point, as well as their sum frequency, while the other peaks are from comb line pairings at different numbers of FSRs away from the SHG fundamental frequency. We note that we need to align the polarizations of both comb lines to the PPLN so that the desired SFG line power is maximized. Both long and short wavelength dispersive waves are involved in the f-2f process to help boost the power. We further amplified the 1 μm light using a semiconductor optical amplifier (SOA) (Innolume), providing a ∼13 dB gain under our operating condition. We insert a 1-nm-wide tunable bandpass filter (Photonwares) after the SOA to suppress the amplified

spontaneous emission (ASE) noise. The powers after the SOA and bandpass filter are measured to be approximately −10 dBm (dispersive wave) and −23 dBm (SFG line closest to dispersive wave) using an optical spectrum analyzer. The f-2f beat is detected via a high-speed PD (Thorlabs DXM30AF, 30 GHz).

Figures 2(f)–2(h) show the detected beat notes for δf_{rep}, f_{Vernier}, and $f_{\mathrm{f-2f}}$ respectively. We are able to achieve a good SNR of ∼50 dB for the f-2f beat at 100 kHz resolution bandwidth (RBW). For this comb pair, the selected comb lines for SFG correspond to $N = 5$, and the Vernier overlap is at $n = 45$. We can obtain the divided repetition rate of our 900 GHz octave-spanning main comb by dividing the f_{Vernier} by 46 and mixing with δf_{rep} to get $f_{\mathrm{rep1}}/46$ [Eq. (4)]. To single out the CEO frequency according to Eq. (7), we first electronically mix the $f_{\mathrm{f-2f}}$ and f_{Vernier} beats for their frequency difference, followed by a programmable divider with a division factor of 5. We mix this divided beat with δf_{rep} so that their frequency difference gives $f_{\mathrm{CEO1}}/5 \approx 19.525$ GHz. The $f_{\mathrm{CEO1}}/5$ beat is further divided by 64 [as shown in Fig. 2(i)] to bring it within the bandwidth of a frequency counter (Keysight 53230A).

In terms of the f-2f beat tunability using the SFG approach, in the experiment, we can make use of $\sim \pm 5$ SFG lines to realize a wide range of $\sim \pm 100$ GHz coverage, which significantly increases the chance for achieving an electronically detectable f-2f beat. The SFG coverage range is constrained mainly by the TDFA gain bandwidth, the power of the microcomb lines at ∼2 μm wavelengths, and the conversion characteristics of the PPLN waveguide.

Next, we conduct measurements to verify the electronically divided f_{rep} and f_{CEO} beats obtained by the Vernier method. Both microcombs are free-running, and their f_{rep} and f_{CEO} are drifting due to environmental fluctuations, pump laser frequency instability, and so on. The verification measurements aim to measure variations in f_{rep} and f_{CEO} and illustrate whether the results from our Vernier approach agree with independent methods.

To verify the Vernier-processed f_{rep}, we use an EO frequency comb, described elsewhere [21]. The EO frequency comb generator produces modulation sidebands at a frequency set by an RF synthesizer, f_{syn}. Here, we input two neighboring comb lines from the main comb. The EO-generated sidebands from the two microcomb lines come close to overlapping at the midpoint between the two soliton lines and produce a detectable beat $f_{\mathrm{EO\,beat}}$. Thus, the repetition rate can be expressed as

$$f_{\mathrm{rep1}} = M_{\mathrm{syn}} \times f_{\mathrm{syn}} \pm f_{\mathrm{EO\,beat}}, \tag{8}$$

where M_{syn} is the number of EO comb lines to span f_{rep1}. The sign of the beat can be found by shifting the EO modulation frequency and observing a resulting positive or negative shift in the beat frequency. For this measurement, we pick two comb lines from the main comb at ∼1534.8 nm and ∼1541.8 nm and send them to the frequency comb generator driven at ∼16.9 GHz. The overlapping sidebands are optically filtered and amplified before sending to a PD. We measure the $f_{\mathrm{EO\,beat}}$ to be 11.225 MHz with a minus sign. Using Eq. (8), the repetition rate is calculated to be 895.54382 GHz, with $M_{\mathrm{syn}} = 53$ and a synthesizer frequency of 16.897265 GHz.

To determine f_{rep1} utilizing the Vernier approach, we divide the f_{Vernier} by 46 and mix it with the δf_{rep} to get a beat at $f_{\mathrm{rep1}}/46$. To reduce the frequency to within the bandwidth of our frequency counter, the beat is further divided by 64, and we measure $f_{\mathrm{rep1}}/2944$ at the counter. Figure 3(a) shows the repetition rate of the main comb measured using the Vernier and EO comb methods simultaneously using two frequency counters at 10 ms gate time. The two methods agree very closely. We note that we have used external trigger and gate signals, generated using arbitrary waveform generators (AWGs, Keysight 33220A and 33600A), to precisely synchronize the counters for the measurement. Furthermore, we have referenced the counters and EO comb synthesizer to a common 10 MHz GPS-disciplined reference to eliminate relative frequency drifting. Figure 3(b) shows Δf_{rep1}, the difference between the repetition rate as measured by the Vernier method and as measured by the EO comb method in Fig. 3(a). The frequency difference is within ±2 kHz, suggesting that the out-of-loop measurement of f_{rep} agrees well with the Vernier method. The f_{rep1} is then measured using the two methods at different counter gate times. We post-process the data to obtain Δf_{rep1} and further calculate the Allan deviation of Δf_{rep1} under various gate times, as shown in Fig. 3(c).

We further investigate whether the accuracy of the Δf_{rep1} measurement is limited by the instruments involved in the experiment. In this case, the instrument limits can come from (1) the limited precision (originated from limited timing resolution) of the frequency counter readings and (2) the stability of the frequency synthesizer driving the EO comb. There are two frequency counters measuring $f_{\mathrm{EO\,beat}}$ and $f_{\mathrm{rep1}}/2944$, where the $f_{\mathrm{rep1}}/2944$ beat with a large division factor results in a much better beat stability and may reach the frequency counter detection limit. The orange dashed line Fig. 3(c) shows the Allan deviation measurement of a stable synthesizer at 304 MHz ($\approx f_{\mathrm{rep1}}/2944$) using the frequency counter. This reveals the frequency counter limit because the actual

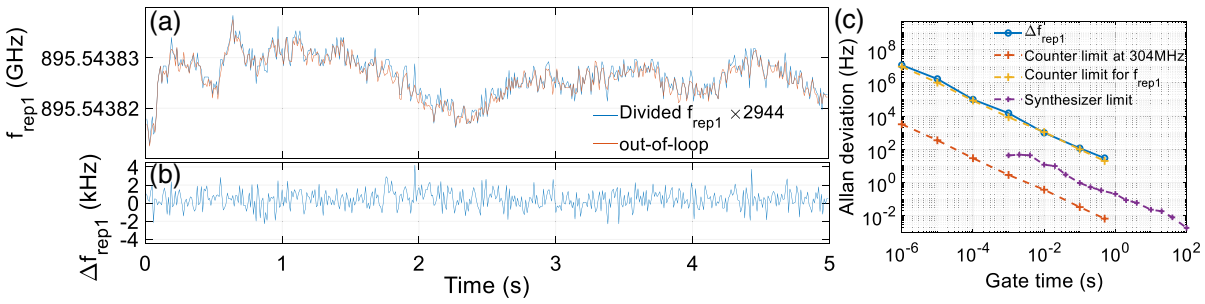

Fig. 3. (a) Repetition rate traces measured by frequency counters using the Vernier method (blue) and the EO comb method (orange) taken at 10 ms gate time. (b) Frequency difference trace between the two measurements. (c) Allan deviations of the frequency difference (blue solid line), the counter resolution limit measured by synthesizer at 304 MHz (orange dashed line), the calculated counter limit for in-loop f_{rep1} (yellow dashed line), and the synthesizer limit (purple dashed line).

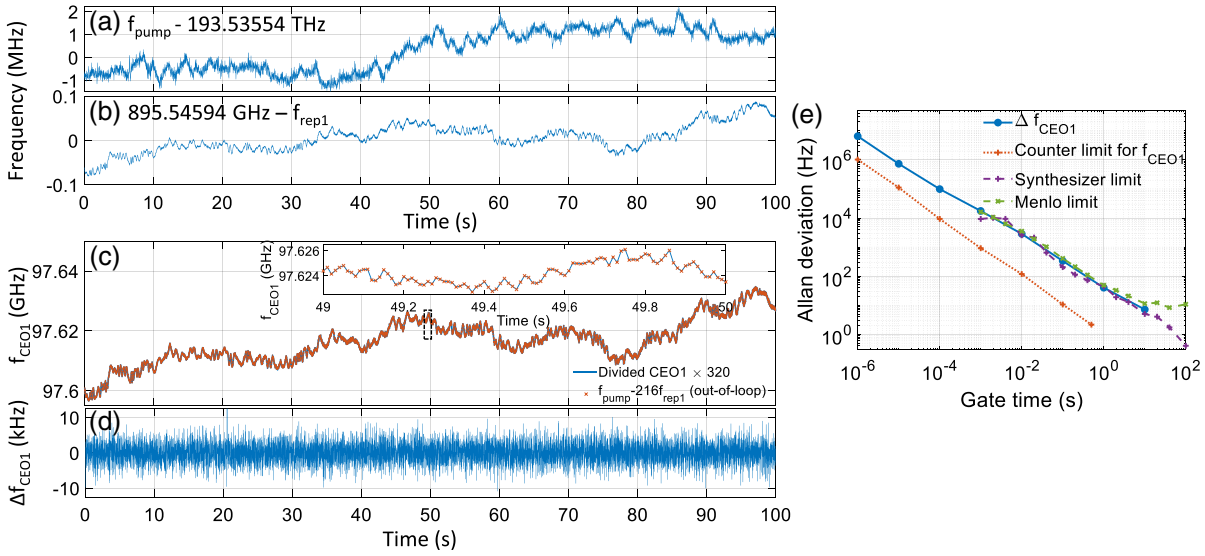

Fig. 4. (a)–(d) Frequency traces for verification of the CEO frequency measurement. (a) f_{pump} obtained by beating the pump frequency with a Menlo comb line. (b) f_{rep1} measured using the EO comb approach. (c) f_{CEO1} measured using the Vernier method (blue) and the out-of-loop verification (orange). Inset, zoom-in view at the dashed region. (d) Frequency difference trace between the two approaches. In (a)–(d), the gate times are 10 ms. (e) Allan deviations of the frequency difference (blue solid line), the counter limit (orange dashed line), the synthesizer limit (purple dashed line), and the Menlo limit (green dashed line).

stability of the synthesizer is better than the counter measurement indicates, a finding confirmed by measuring the same synthesizer on a phase noise test set (PNTS) (Microsemi 5125A) with better measurement precision than the counter (shown in Supplement 1). When multiplied by a factor of 2944 (the divisor of f_{rep1} for the Vernier measurement), we get the yellow dashed line, which is very close to the experimental data. We also analyze the contribution of the synthesizer used to generate the EO comb in the Δf_{rep1} measurement by estimating the Allan deviation of $M_{\text{syn}} \times f_{\text{syn}}$ using the Allan deviation of the synthesizer measured at 304 MHz by PNTS. The purple dashed line in Fig. 3(c) shows the resulting synthesizer limit, which is lower than the frequency counter limit. This suggests that the difference between the Vernier-comb-based repetition rate measurement and the out-of-loop EO comb measurement is limited by the frequency counter, which validates our Vernier measurement. We conclude that we have successfully divided an octave-spanning comb's ∼THz repetition rate to detectable frequencies.

Next, we validate the CEO frequency measurement from the Vernier approach using a similar measurement. The experimental setup can be found in Supplement 1. The verification requires measuring the pump frequency f_{pump} and the repetition rate of the main comb f_{rep1} simultaneously. The pump frequency can be measured in real time by beating the pump laser against a mode of a stable commercial fiber-based frequency comb (Menlo Systems) to generate $f_{\text{pump beat}}$. The repetition rate can again be measured with an external EO comb. Given these two simultaneous measurements, we acquire the CEO frequency through

$$\begin{aligned} f_{\text{CEO1}} &= f_{\text{pump}} - m_1 \times f_{\text{rep1}} \\ &= f_{\text{pump}} - m_1 \times (M_{\text{syn}} \times f_{\text{syn}} \pm f_{\text{EO beat}}), \end{aligned} \tag{9}$$

where m_1 is the mode number of the pump, which is 216 in our case. f_{syn} is the EO comb synthesizer frequency, and M_{syn} is the EO comb mode number [see Eq. (8)]. The Menlo system has a precisely set 250 MHz repetition rate $f_{\text{rep,Menlo}}$ and a −20 MHz offset frequency $f_{\text{CEO,Menlo}}$. The pump frequency can thus be obtained using

$$f_{\text{pump}} = M_{\text{Menlo}} \times f_{\text{rep,Menlo}} + f_{\text{CEO,Menlo}} \pm f_{\text{pump beat}}, \tag{10}$$

where the mode order M_{Menlo} can be found through a wavemeter measurement of the pump frequency, and the ± sign is determined by increasing or decreasing the f_{pump} to observe the $f_{\text{pump beat}}$ change.

We use three frequency counters synchronized with common external trigger and gate signals to simultaneously measure the divided CEO frequency $f_{\text{CEO1}}/320$, $f_{\text{pump beat}}$, and $f_{\text{EO beat}}$. The three counters, EO comb synthesizer, and Menlo comb are all again synchronized to a common GPS-disciplined reference to eliminate relative drifting. We obtain f_{CEO1} from the Vernier method [see Eq. (7)] and f_{pump} and f_{rep1} from the verification measurements. Figures 4(a) and 4(b) show the traces of f_{pump} and f_{rep1}, respectively, derived from the frequency counter measurement upon 10 ms gate time. Figure 4(c) shows the f_{CEO1} measured from the Vernier method and the verification measurement, which overlay on each other exactly (the inset shows a 1 s zoomed-in plot of the two traces), suggesting an excellent agreement between these two methods. The difference between these two measurements Δf_{CEO1} is within ±10 kHz, as shown in Fig. 4(d). We conduct measurements at various gate times for the three frequency counters to observe the Δf_{CEO1}. The Allan deviation of Δf_{CEO1} under different gate time is plotted in Fig. 4(e).

We investigate the instrumentation limits of our validation measurement. Possible contributing elements include the three frequency counters' respective resolution limits, the stability of the Menlo comb line against which f_{pump} is measured, and the frequency synthesizer driving the EO comb with which f_{rep1} is measured. The three frequency counters measuring $f_{\text{CEO1}}/320$, $f_{\text{pump beat}}$, and $f_{\text{EO beat}}$ are identical, implying the same resolution limit on each measurement. However, importantly, to bring f_{pump} and f_{rep1} into the bandwidth of our counters, they are downmixed

with a Menlo comb system and an EO comb system, respectively. By reducing the carrier frequency without reducing the frequency fluctuations, this downmixing allows the counters to directly and precisely measure the stability of these two signals. By contrast, the third counter measures $f_{CEO1}/320$. This signal is brought into the bandwidth of the counter using frequency division, which reduces both the carrier frequency and, critically, also the frequency fluctuations. As a consequence, the signal's frequency fluctuations are brought closer to the third counter's resolution limit and, hence, are not as precisely resolved as those of the other two signals. The third counter's resolution limit dominates the contributions of the other two counters toward the f_{CEO} validation measurement as a result and is shown as the orange dashed line in Fig. 4(e). However, compared to other contributions explained in the next paragraph, the frequency counters do not impose the primary limit to the frequency imprecision in our CEO frequency measurements.

We then photodetect our Menlo comb and send the repetition rate to the PNTS, referenced to our common GPS-disciplined clock, for stability measurement. We post-process by multiplying the resulting absolute Allan deviation with the mode number of the tooth nearest to our pump laser ($\approx 774,140$) to convert to an estimated optical stability. Here we neglect the noise contributed by $f_{CEO,Menlo}$ as it is quite small by comparison, and we cannot simultaneously measure $f_{CEO,Menlo}$ and $f_{rep,Menlo}$ with sufficient stability given our current laboratory equipment. Finally, the EO comb frequency synthesizer contribution in the Δf_{CEO1} measurement is analysed by calculating the Allan deviation of $m_1 \times M_{syn} \times f_{syn}$ for deriving Δf_{CEO1} [see Eq. (9)]. We measure the fractional Allan deviation of the synthesizer using PNTS. Multiplying by $216 \times 53 \times 16.9$ GHz, we obtain the Allan deviation of the synthesizer limit plotted in Fig. 4(e) with purple dashed line. The resulting up-scaled Allan deviations of the synthesizer (purple dashed line) and Menlo comb line (green dashed line) are in close agreement with one another, suggesting they are multiplying up the common 10 MHz GPS-disciplined reference with similar stability levels. Furthermore, they predict the Δf_{CEO} Allan deviation very well as Fig. 4(e) shows. This indicates that the synthesizer and Menlo comb in our verification setup limit the experiment. Thus, we conclude that our novel Vernier method of dividing f_{CEO} has been verified to the limits of our measurement apparatus.

4. DISCUSSION AND CONCLUSION

In summary, we have demonstrated a dual-comb Vernier system for frequency division of repetition rates around ~900 GHz. In principle, we are able to divide the repetition rates of both our combs, but most critically that of our octave-spanning main comb, which features strong dispersive waves (especially at the short wavelength) and is a good candidate for self-referencing. Furthermore, using the combination of our two broadband Vernier combs, we have demonstrated detection of a ~100 GHz f_{CEO} via SFG to obtain a modified f-2f beat well within the bandwidth of commercial PDs. We have attained a frequency-divided f_{CEO} below 20 GHz, which is compatible with typical electronic components. The simultaneous ability to divide down both the repetition rate and f_{CEO} of our main comb, both normally undetectable, suggests that this Vernier dual-comb technique could prove to be a valuable tool for generating fully stabilized on-chip frequency comb systems for a variety of applications.

Our method relies on frequency-shifting f_{CEO1} by $N\delta f_{rep}$ to derive a modified f-2f beat. The range of N largely depends on the main and Vernier comb parameters (such as comb line power at 2 μm and Vernier overlap position). The comb pair used here allows us to detect f_{CEO1} of $\pm \sim 100$ GHz (with N ranging from −5 to 5). $N = 0$ corresponds to the Vernier overlap frequency around 1956 nm, and $N = \pm 5$ corresponds to ~1902 nm and ~2015 nm on the short and long wavelength side, respectively. To extend the f_{CEO} detection range beyond a 200 GHz range, one should increase the values of N, currently limited by roll-off in the optical power spectra. For example, with modified dispersion engineering, one can attempt to shift the long wavelength dispersive waves further beyond 2 μm (the comb spectrum falls off rapidly beyond the long wavelength dispersive wave). It may also be helpful to bring in additional fiber amplifiers (e.g., TDFA's can be configured for shorter wavelength operation below 1900 nm; holmium-doped fiber amplifiers can go well beyond 2 μm). Moreover, using 2 μm single-mode fibers to deliver the longer wavelength light to the nonlinear crystal would avoid the higher optical loss associated with 1.55 μm single-mode fibers (which are currently used throughout our setup). In addition, a nonlinear crystal with higher conversion efficiency, which may be achievable based on developments in low-loss waveguide technology in thin-film lithium niobate [22,23], would also help.

Funding. Defense Advanced Research Projects Agency (APhI program); Air Force Office of Scientific Research (FA9550-20-1-0283); Vetenskapsrådet (VR 2020-00453); King Saud University, Researchers Supporting Project (RSPD2023R613).

Acknowledgment. The effort at Purdue under the DARPA APhI program was part of a project team lead by Sandia National Laboratories. The Si_3N_4 fabrication has been done at Myfab Chalmers. The authors thanks Beichen Wang, Scott Diddams, Scott Papp, and Jonah Quirk for helpful discussions, Keysight for the use of a frequency counter, Ryan Schneider for assistance with PPLN crystal characterization, and Mohammad Abu Khater and Mike Kickbush for assistance with RF filtering. Portions of this work were submitted to CLEO 2023. Some of our early work on Vernier dual combs, such as dual-octave comb pairs, was presented at CLEO 2021 (SW2H.7) and CLEO 2022 (SW4O.2).

Disclosures. The authors declare no conflicts of interest.

Data availability. Data underlying the results of this study are available at [24].

Supplemental document. See Supplement 1 for supporting content.

REFERENCES

1. S. A. Diddams, T. Udem, J. C. Bergquist, E. A. Curtis, R. E. Drullinger, L. Hollberg, W. M. Itano, W. D. Lee, C. W. Oates, K. R. Vogel, and D. J. Wineland, "An optical clock based on a single trapped ^{199}Hg+ ion," Science **293**, 825–828 (2001).
2. N. Hinkley, J. A. Sherman, N. B. Phillips, M. Schioppo, N. D. Lemke, K. Beloy, M. Pizzocaro, C. W. Oates, and A. D. Ludlow, "An atomic clock with 10^{-18} instability," Science **341**, 1215–1218 (2013).
3. X. Xie, R. Bouchand, D. Nicolodi, M. Giunta, W. Hänsel, M. Lezius, A. Joshi, S. Datta, C. Alexandre, M. Lours, P.-A. Tremblin, G. Santarelli, R. Holzwarth, and Y. L. Coq, "Photonic microwave signals with zeptosecond-level absolute timing noise," Nat. Photonics **11**, 44–47 (2017).
4. R. Holzwarth, T. Udem, T. W. Hänsch, J. Knight, W. Wadsworth, and P. St. J. Russell, "Optical frequency synthesizer for precision spectroscopy," Phys. Rev. Lett. **85**, 2264–2267 (2000).
5. I. Coddington, W. C. Swann, L. Nenadovic, and N. R. Newbury, "Rapid and precise absolute distance measurements at long range," Nat. Photonics **3**, 351–356 (2009).
6. I. Coddington, N. Newbury, and W. Swann, "Dual-comb spectroscopy," Optica **3**, 414–426 (2016).

7. A. J. Metcalf, T. Anderson, C. F. Bender, *et al.*, "Stellar spectroscopy in the near-infrared with a laser frequency comb," Optica **6**, 233–239 (2019).
8. S. A. Diddams, K. Vahala, and T. Udem, "Optical frequency combs: coherently uniting the electromagnetic spectrum," Science **369**, eaay3676 (2020).
9. D. J. Jones, S. A. Diddams, J. K. Ranka, A. Stentz, R. S. Windeler, J. L. Hall, and S. T. Cundiff, "Carrier-envelope phase control of femtosecond mode-locked lasers and direct optical frequency synthesis," Science **288**, 635–639 (2000).
10. T. J. Kippenberg, A. L. Gaeta, M. Lipson, and M. L. Gorodetsky, "Dissipative Kerr solitons in optical microresonators," Science **361**, eaan8083 (2018).
11. P. Del'Haye, A. Coillet, T. Fortier, K. Beha, D. C. Cole, K. Y. Yang, H. Lee, K. J. Vahala, S. B. Papp, and S. A. Diddams, "Phase-coherent microwave-to-optical link with a self-referenced microcomb," Nat. Photonics **10**, 516–520 (2016).
12. Q. Li, T. C. Briles, D. A. Westly, T. E. Drake, J. R. Stone, B. R. Ilic, S. A. Diddams, S. B. Papp, and K. Srinivasan, "Stably accessing octave-spanning microresonator frequency combs in the soliton regime," Optica **4**, 193–203 (2017).
13. M. H. Pfeiffer, C. Herkommer, J. Liu, H. Guo, M. Karpov, E. Lucas, M. Zervas, and T. J. Kippenberg, "Octave-spanning dissipative Kerr soliton frequency combs in Si_3N_4 microresonators," Optica **4**, 684–691 (2017).
14. D. T. Spencer, T. Drake, T. C. Briles, *et al.*, "An optical-frequency synthesizer using integrated photonics," Nature **557**, 81–85 (2018).
15. Z. L. Newman, V. Maurice, T. Drake, *et al.*, "Architecture for the photonic integration of an optical atomic clock," Optica **6**, 680–685 (2019).
16. T. E. Drake, T. C. Briles, J. R. Stone, *et al.*, "Terahertz-rate Kerr-microresonator optical clockwork," Phys. Rev. X **9**, 031023 (2019).
17. B. Wang, Z. Yang, X. Zhang, and X. Yi, "Vernier frequency division with dual-microresonator solitons," Nat. Commun. **11**, 3975 (2020).
18. Z. Ye, K. Twayana, P. A. Andrekson, and V. Torres-Company, "High-Q Si_3N_4 microresonators based on a subtractive processing for Kerr nonlinear optics," Opt. Express **27**, 35719–35727 (2019).
19. G. Moille, Q. Li, T. C. Briles, S.-P. Yu, T. Drake, X. Lu, A. Rao, D. Westly, S. B. Papp, and K. Srinivasan, "Broadband resonator-waveguide coupling for efficient extraction of octave-spanning microcombs," Opt. Lett. **44**, 4737–4740 (2019).
20. J. R. Stone, T. C. Briles, T. E. Drake, D. T. Spencer, D. R. Carlson, S. A. Diddams, and S. B. Papp, "Thermal and nonlinear dissipative-soliton dynamics in Kerr-microresonator frequency combs," Phys. Rev. Lett. **121**, 063902 (2018).
21. A. J. Metcalf, V. Torres-Company, D. E. Leaird, and A. M. Weiner, "High-power broadly tunable electrooptic frequency comb generator," IEEE J. Sel. Top. Quantum Electron. **19**, 231–236 (2013).
22. C. Wang, C. Langrock, A. Marandi, M. Jankowski, M. Zhang, B. Desiatov, M. M. Fejer, and M. Lončar, "Ultrahigh-efficiency wavelength conversion in nanophotonic periodically poled lithium niobate waveguides," Optica **5**, 1438–1441 (2018).
23. J. Lu, J. B. Surya, X. Liu, A. W. Bruch, Z. Gong, Y. Xu, and H. X. Tang, "Periodically poled thin-film lithium niobate microring resonators with a second-harmonic generation efficiency of 250,000%/w," Optica **6**, 1455–1460 (2019).
24. K. Wu, N. P. O'Malley, S. Fatema, C. Wang, M. Girardi, M. S. Alshaykh, Z. Ye, D. E. Leaird, M. Qi, V. Torres-Company, and A. M. Weiner, "Raw data for Vernier Microcombs For High-Frequency Carrier Envelope Offset and Repetition Rate Detection," Zenodo, 2023, https://doi.org/10.5281/zenodo.7843860.